A Small Disturbance, But a Serious Disease: The Possible Mechanism of D52H-Mutant of Human PRS1 That Causes Gout

ARTICLE *in* INTERNATIONAL UNION OF BIOCHEMISTRY AND MOLECULAR BIOLOGY LIFE · JUNE 2013

Impact Factor: 3.14 · DOI: 10.1002/iub.1154 · Source: PubMed

5 AUTHORS, INCLUDING:

Maikun Teng
University of Science and Technology of China
138 PUBLICATIONS **1,548** CITATIONS
SEE PROFILE

Xu Li
University of Science and Technology of China
58 PUBLICATIONS **379** CITATIONS
SEE PROFILE

Research Communication

A Small Disturbance, But a Serious Disease: The Possible Mechanism of D52H-Mutant of Human PRS1 That Causes Gout

Peng Chen[1,2]
Jianzhong Li[3]
Jin Ma[4]
Maikun Teng[1,2]*
Xu Li[1,2]

[1]University of Science and Technology of China, School of Life Sciences, Hefei, Anhui, People's Republic of China
[2]Chinese Academy of Sciences, Key Laboratory of Structural Biology, Hefei, Anhui, People's Republic of China
[3]Department of Otolaryngology Head and Neck Surgery, Fuzhou General Hospital of Nanjing Command, PLA., Fuzhou, Fujian, People's Republic of China
[4]Department of Geriatrics, The First People's Hospital of Hefei, Hefei, Anhui, People's Republic of China

Abstract

Phosphoribosyl pyrophosphate synthetase isoform 1 (PRS1) has an essential role in the *de novo* and salvage synthesis of human purine and pyrimidine nucleotides. The dysfunction of PRS1 will dramatically influence nucleotides' concentration in patient's body and lead to different kinds of disorders (such as hyperuricemia, gout and deafness). The D52H missense mutation of PRS1 will lead to a conspicuous phosphoribosyl pyrophosphate content elevation in the erythrocyte of patients and finally induce hyperuricemia and serious gout. In this study, the enzyme activity analysis indicated that D52H-mutant possessed similar catalytic activity to the wild-type PRS1, and the 2.27 Å resolution D52H-mutant crystal structure revealed that the stable interaction network surrounding the 52 position of PRS1 would be completely destroyed by the substitution of histidine. These interaction variations would further influence the conformation of ADP-binding pocket of D52H-mutant and reduced the inhibitor sensitivity of PRS1 in patient's body.

Keywords: *PRS1; gout; mutation; crystal structure; superactivity*

Introduction

Human phosphoribosyl pyrophosphate synthetase (PRS, EC 2.7.6.1) is one of the essential enzymes in the purine nucleotides metabolic pathway, which catalyzes the synthesis of phosphoribosyl pyrophosphate (PRPP) from adenosine triphosphate and ribose 5-phosphate (R5P) (1). It belongs to class I PRS family, which requires Mg^{2+} and inorganic phosphate (Pi) for enzymatic activity, but can be inhibited allosterically by ADP and possibly other nucleotides (2). Human PRS has three isoforms that share very high sequence identity (95.0% between PRS1 and PRS2; 94.3% between PRS1 and PRS3 and 91.2% between PRS2 and PRS3, respectively). *PRS1* and *PRS2* genes are located on the *X* chromosome and are expressed in a wide range of tissues, but *PRS3* is an autosomal gene expressed specifically in testis (3). Unlike the isoenzymes in lower eukaryotes, each human PRS1, PRS2 and PRS3 can perform their catalytic functions, respectively. As far as we are concerned, no report indicated that they could cooperate to form any functional heteropolymer with each other.

PRPP is essential for the *de novo* synthesis of purine, pyrimidine, and pyridine nucleotides (Fig. 1) (4). During the first step of purine synthesis, PRPP is used as a substrate for PRPP amidotransferase to produce purine nucleotides such as

Abbreviations: *PRS1 phosphoribosyl pyrophosphate synthetase isoform 1 PRPP phosphoribosyl pyrophosphate ITC isothermaltitration calorimetry rmsd root mean-square deviation*

Volume 65, Number 6, June 2013, Pages 518–525

**Address for correspondence to: Maikun Teng, University of Science and Technology of China, School of Life Sciences, Hefei, Anhui 230026, People's Republic of China, Fax: +86-551-3607334. E-mail: sachem@ustc.edu.cn.*
**Present address: Chinese Academy of Sciences, Key Laboratory of Structural Biology, Hefei, Anhui 230026, People's Republic of China.*

Received 14 January 2013; accepted 31 January 2013
DOI: 10.1002/iub.1154
Published online 18 March 2013 in Wiley Online Library (wileyonlinelibrary.com)

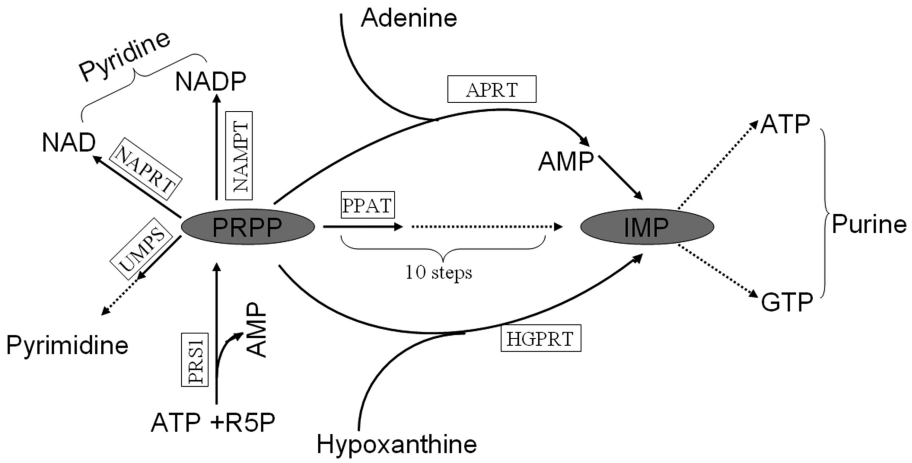

FIG 1 *PRPP is an essential substrate for several important products synthesis. Solid line represents one-step reaction, whereas dotted line represents one step at least. The curve is special for purine salvage synthesis pathway, whereas the 10-step reactions are for purine* de novo *synthesis.*

adenosine triphosphate (ATP) and guanosine triphosphate (GTP). This step serves specifically as the rate-limiting reaction for purine nucleotide synthesis *in vivo*. (5). PRPP is also essential for pyrimidine nucleotide synthesis. PRPP acts as cofactor for uridine monophosphate synthetase (UMPS) that converts orotic acid into UMP (the precursor of all pyrimidine nucleotides) (6). Finally, PRPP is utilized for pyridine nucleotide synthesis by nicotinate phosphoribosyl transferase and nicotinamide phosphoribosyl transferase. The two enzymes can add a ribonucleotide moiety to nicotinic acid or nicotinamide to produce the important cofactors nicotinamide adenine dinucleotide (NAD) or nicotinamide adenine dinucleotide phosphate (NADP), respectively (7). PRPP is not only utilized for the *de novo* synthesis of purine, pyrimidine and pyridine nucleotides, but also utilized for the salvage pathway by hypoxanthine guanine phosphoribosyltransferase and adenine phosphoribosyltransferase. Accordingly, mutations in PRS, which influence generation rate and concentration of PRPP, may affect vital cell functions, such as nucleic acid synthesis, energy metabolism and cellular signaling.

In contrast to human PRS1, PRS2 and PRS3 have not been implicated in disease. Human PRS1 missense mutations can lead to four kinds of syndromes, such as PRS1 superactivity (8), Charcot–Marie–Tooth disease-5 (CMTX5) (9), Arts syndrome (10) and X-linked nonsyndromic sensorineural deafness (DFN2) (11) (Table 1). During the last 40 years, seven PRS1 gain-of-function single-base missense mutations had been indicated to be associated with excessive uric acid production and hereditary gout (13), and eight loss-of-function single-base missense mutations of PRS1 had been indicated to be associated with congenital sensorineural hearing impairment (15, 16, 19, 20). Recently, one novel missense mutation of PRS1 in a patient was identified, which showed the uric acid overproduction without gout but with developmental delay,

TABLE 1 ***Different version of human PRS1 mutations that cause disorders***

Human disorder	*Amino acid change*	*Activity change*	*Year and reporters*
PRS1 superactivity	N114S D182H	Gain of function	Roessler et al. (*12*)
PRS1 superactivity	D52H L129I A189V H192Q	Gain of function	Becker et al. (*13*)
PRS1 superactivity	H192L	Gain of function	Garcia-Pavia et al. (*14*)
Arts Syndrome	Q133P L152P	Loss of function	de Brouwer et al. (*15*)
CMTX5	E43D M115T	Loss of function	Kim et al. (*16, 17*)
DFN2	D65N A87T I290T G306R	Loss of function	Liu et al. (*17*)
PRS superactivity and Arts syndrome	V142L	Intermediate phenotype between the two mentioned above	Moran et al. (*18*).

hypotonia, hearing loss and recurrent respiratory infections. Combined these syndromes together, the patient had an intermediate phenotype which was characterized by both the gain-of-function PRS1 superactivity and the loss-of-function Arts syndrome (18).

D52H mutation was first discovered in a case report in which two brothers suffered from gouty arthritis and recurrent bilateral uric acid lithiasis since they were about 20 years old (8). Kinetic analysis indicated that this family possessed PRPP synthetase superactivity defect, which was correctly attributed to altered allosteric regulation of PRS1 by purine nucleotide inhibitors and Pi (21). The mutation accounting for the enzyme kinetic abnormalities and the ensuing alterations in cellular physiology (increased PRPP concentrations and rates of generation) (8) and *in vivo* clinical manifestations (gout and uric acid urolithiasis resulting from hyperuricemia and uric acid overproduction) (21) was defined in 1995 as substitution of His for Asp in residue 52 of human PRS1 (13).

Although the genetic and functional basis of PRS1 superactivity of D52H-mutant has been fully discussed, the direct structural–catalytic mechanism bases of the purine nucleotide feedback-resistant of D52H-mutant are still unknown. In this study, we attempt to extend information about D52H-related PRPP synthetase aberration to the details of altered catalysis and regulation as they are affected by the His for Asp substitution by structural biology method. The 2.27-Å resolution crystal structure of PRS1 D52H-mutant reveals an overall structure, resembling that of wild-type PRS1 (wt-PRS1), whereas the stable interaction network surrounding the 52 position is completely destroyed by the substitution of histidine. These interaction variations further influence the conformation of ADP-binding pocket and reduce the inhibitor-binding affinity of D52H-mutant.

Materials and Methods

Cloning, Protein Expression and Purification

Gene of wt-PRS1 (NCBI entry code, 5631) was amplified from the human cDNA library, and primers used in cloning were synthesized by Invitrogen (Shanghai, China). wt-PRS1 gene was cloned into the NdeI and XhoI sites of pET22b(+) vector (Novagen) with a His_6 tag (LEHHHHHH) at the C-terminus of wt-PRS1, and the plasmid was transformed into *Escherichia coli* BL21(DE3) (Merck) for protein expression. The cells were induced with 0.25 mM isopropyl-β-D-thiogalactoside at 289 K for 20 h when OD_{600} reached 0.6. Cells were harvested and disrupted by sonication in buffer A (50 mM Tris-HCl, pH 8.5, 400 mM NaCl and 10% glycerol), and the protein was purified by Ni-chelating resin (GE Healthcare, Waukesha, WI, USA) and gel filtration using a HiLoad 16/60 Superdex 200 column (GE Healthcare, Waukesha, WI, USA). The purified protein showed a single band in SDS-PAGE at ~35 kDa, consistent with the expected molecular weight (data not shown). The plasmid of D52H-mutant was generated from the recombinant wt-PRS1 pET22b (+) vector by site-directed mutagenesis from G to C at position 154 (TaKaRa MutanBEST Kit). Mutant protein was purified using the same procedure as that for the wild-type protein.

Crystallization, Data Collection, Structure Determination and Model Refinement

Crystals of PRS1 D52H-mutant were obtained at 285 K by vapor diffusion of 2 mg/mL of protein against a reservoir of 1.9 M ammonium sulfate, 1 mM magnesium chloride and 0.1 M sodium citrate, pH 4.1, after 3 days.

A crystal mounted in a loop was soaked briefly in a cryoprotectant solution consisting of the corresponding reservoir solution supplemented with 25% v/v glycerol, and then flash-cooled in liquid nitrogen. X-ray diffraction data were collected on beamline 17U1 of the Shanghai Synchrotron Radiation Facility (SSRF) using a Jupiter CCD detector. All frames were collected at 100 K using an oscillation angle of 1° with an exposure time of 1 s per frame. The crystal-to-detector distance was set to 180 mm. The complete diffraction data set was subsequently processed using *HKL-2000* (22) and programs in the *CCP4 package* (23).

The structure was solved with the molecular replacement method to a resolution of 2.27 Å using the human wt-PRS1 (PDB entry 2H06) (3) as the search models in *MOLREP* in the *CCP4 package* (23). Refinement was performed by *REFMAC5* (24) and *PHENIX* (25). Between each round of refinement, the model was fitted to the $2F_o - F_c$ electron-density map with the program *Coot* (26). The final refined model has an *R*-factor (R_{free}) of 17.8% (23.3%). The quality of final model was checked with *PROCHECK* (27). Data collection and structure refinement statistics are summarized in Table 2. The 2.27-Å structure of human PRS1 D52H-mutant has been deposited with the RCSB Protein Data Bank (http://www.rcsb.org) under accession code 4F8E. All figures were prepared using PyMOL (Schrödinger).

Enzyme Activity Analysis

Both wt-PRS1 and D52H-mutant were assayed with three different concentrations of PRS1 inhibitor ADP (0, 0.15 and 0.25 mM). Each reaction was carried out as follows: 100 μL protein was incubated for 30 min at 310 K with 100 μL reaction mixture containing: 50 mM Tris-HCl, pH 7.4, 7 mM $MgCl_2$, 1 mM EDTA, 1 mM DTT, 32 mM NaPi, saturating concentrations of the substrates ATP (0.5 mM) and ribose 5-phosphate (0.15 mM). On completion of the incubation, the reaction was terminated by the addition of 200 μL of 10% trichloroacetic acid. After centrifugation (10,000g at 277 K for 20 min), 10 μL of the supernatant (adjusted to pH 7.0) was subjected to ion-pair HPLC (Agilent Eclipse XDB-C18, 5 μm, 4.6 mm × 150 column) to separate the AMP, eluted at 295 K with a mixture of 24% v/v methanol and 50 mM KH_2PO_4, pH 5.8, at a flow rate of 0.75 mL/min. Absorbance change was measured at 259 nm. All the values were the average of three measurements. The specific activity (units/mg of protein) of PRS1 is defined as an increase of AMP (nmol) generated by per milligram of PRS1 per hour.

TABLE 2 *Data collection and refinement statics*

Data collection statistics	
Space Group	*H* 3
Wavelength (Å)	0.9784
Unit cell parameters (Å,°)	$a = 170.31$, $b = 170.31$, $c = 61.75$ Å, $\alpha = \beta = 90^{\circ}$, $\gamma = 120^{\circ}$
Resolution limits (Å)[a]	50–2.27 (2.31–2.27)
R_{merge} (%)[b]	8.0 (62.6)
I/σ (I)	24.6 (2.1)
Completeness (%)	99.9 (98.5)
Redundancy	3.8
Refinement statistics	
Number of reflections used	29,053
R_{work}[c]/R_{free} (%)	17.8/23.25
rmsd Bond (Å)	0.008
rmsd Angle (°)	1.15
B-value (Å^2)	35.29
Ramachandran plot	
Most favored (%)	94.6
Additional allowed (%)	5.4

[a] *Values in parentheses are for the highest resolution shell.*
[b] $R_{merge} = \Sigma_{hkl}\ \Sigma i |Ii(hkl) - I(hkl)> |/\Sigma hkl\ \Sigma i Ii(hkl)$.
[c] $R_{work} = \Sigma_{hkl} |Fobs| - |Fcalc| / \Sigma hkl |Fobs|$.

The Binding Capacity Measurements for ADP

All isothermal titration calorimetry (ITC) studies were performed with a VP-ITC MicroCal titration calorimeter (Thermo Fisher Scientific, San Jose, CA). Wt-PRS1 and D52H-mutant were dialyzed in buffer B (50 mM Tris-HCl, pH 8.0, 7 mM $MgCl_2$, 400 mM NaCl and 10% glycerol) and were incubated with six-times-higher ATP for 30 min to saturate ATP-binding pocket before titration. The ligand ADP was directly titrated into the reaction cell that contained the control group (PRS1) or working group (D52H-mutant) by the syringe. In total, 34 drops of ligand, each of which had a volume of 8 μL and lasted for 16 s, were titrated into the reaction cell. There was a 220-s spacing between each drop. The final data were fitted by MicroCal Origin software version 7.0 (Thermo Fisher Scientific, San Jose, CA). After reference group being subtracted from the working group, the one-site model was used to fit the final ITC data.

Results and Discussion

Proteins Expression, Purification and Catalytic Activity

Both the purified wt-PRS1 and the D52H-mutant proteins showed a major protein-staining band of 35 kDa on SDS-PAGE (data not shown), in good agreement with the calculated value of 34.8 kDa. The specific activity of D52H-mutant indicated no significant difference with that of wt-PRS1 (Fig. 2A), which was coincident with the enzymatic kinetic result of the recombinant D52H-mutant with reduced apparent molecular mass (~33.8 kD) (13). It indicates that the clinical superactivity of PRS1 D52H-mutant is not primarily based on the improvement of enzyme catalytic ability.

Overall Structure of the D52H-Mutant

To further understand the pathogenic mechanism of D52H-mutant, a 2.27-Å resolution crystal structure of PRS1 D52H-mutant was solved. The tertiary structure of D52H-mutant indicates a homodimer composed of two identical monomers in an asymmetric unit (Fig. 2B), with the crystallographic statistics summarized in Table 2. D52H-mutant consists of two domains with a similar sandwich-like α/β structure. At the N-terminal domain, the central five-stranded parallel β-sheet is surrounded by four α-helices and one 3_{10}-helix; at the C-terminal domain, it is flanked by two α-helices on one side and three α-helices on the other (Fig. 2C). The region from Arg^{196} to Arg^{204} of D52H-mutant is missing in the electron density map. To confirm whether this region is proteolyzed during crystallization, some D52H-mutant crystals were washed twice by reservoir solution and redissolved to be analyzed by electrophoresis. SDS-PAGE analysis indicated that no degradation happened during the crystallization process (data not shown), and it suggested that this region is either highly flexible or has multiple conformations in crystals.

In D52H-mutant, the Asp^{52} of PRS1 is successfully substituted by His^{52}, which confirmed by both the DNA sequencing and the electron density map (Fig. 3A). Structural comparison indicates that the overall structure of D52H-mutant is very similar to that of wt-PRS1 (an root mean-square deviation [rmsd] of 0.179 Å compared with the wt-PRS1 structure 3OZN on C_α positions for 520 residues). Notably, there was no apparent structural difference between the substrate-binding pockets and key catalytic regions of D52H-mutant and wild type, which is well consistent with the results of enzymatic activity assay.

Structural Deviations Between wt-PRS1 and D52H-Mutant

In the wt-PRS1 structure, Asp^{52} strongly interacts with Arg^{84} via a pair of main-chain hydrogen bonds and a side-chain salt bridge (which is actually a combination of hydrogen bonding and an ionic interaction). Asp^{52} also makes side-chain hydrogen bond interactions with Tyr^{54} and His^{304} (on the C-terminal α-helix: Ser^{293}–Asn^{305}). At the same

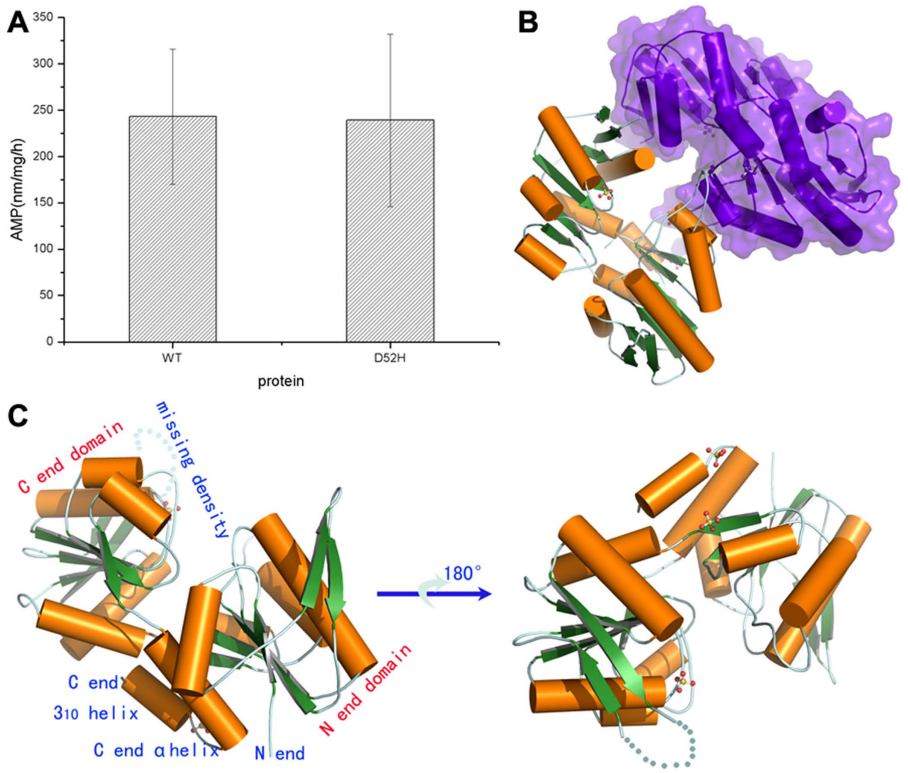

FIG 2 *(A) Specific activity of the wt-PRS1 and D52H mutant. (B) Crystal structure of D52H mutant shows as a dimer in one asymmetry unit. Ribbon representation with α-helices is shown in orange and β-sheets in green. Surface representation of another monomer is shown in magenta. (C) Structure of D52H-mutant monomer and its 180° rotation. Domain composition is shown as labeled in this figure. [Color figure can be viewed in the online issue, which is available at wileyonlinelibrary.com.]*

time, Arg^{84} forms hydrogen bonds with the main-chain nitrogen of Thr^{303} (on the C-terminal α-helix), and some water molecules are involved in above interaction network (Fig. 3B). After the electronegativity, Asp^{52} was substituted by the electropositive histidine in D52H-mutant and stable interaction network was completely destroyed. His^{52} connects only with Ser^{83} via a side-chain hydrogen bond. The free side chain of Arg^{84} deviates away from the His^{52}, and the interaction between the Arg^{84} and the C-terminal α-helix does not exist in D52H-mutant structure (Figs. 3C and 3D). Above interaction deviations do not apparently change the relative positions of other original Asp^{52} interaction partners, but the position correlations between β-strands (βA: Glu^{51}–Val^{56} and βB: Arg^{84}–Ile^{89}) and C-terminal α-helix have been eliminated in D52H-mutant (Fig. 3E).

We also focused that, because of the disappearance of the above structural constraints, some small structural trend alteration and displacement occurred in the loop region from the beginning of His^{304} and the following C-terminal 3_{10} helix (Val^{309}–Phe^{313}) in D52H-mutant structure. Both the sequence alignment between human PRS1 and *Bacillus subtilis* phosphoribosyl pyrophosphate synthetase (bsKPRS) (Fig. 4), and the structural superimposition between wt-PRS1 and bsKPRS–ADP complex (PDB code, 1DKU) with an rmsd of 0.846 Å on C_α positions for 509 residues (28) indicate that the C-terminal 3_{10} helix is responsible for the inhibitor ADP binding in the PRS1 catalytic activity negative-feedback regulation process. For the above reasons, we hypothesized that the substitution of Asp^{52} by His^{52} eliminated the structural constraints between β-strands (βA: Glu^{51}–Val^{56} and βB: Arg^{84}–Ile^{89}) and C-terminal α-helix, and slightly altered the conformation of the following loop region and C-terminal 3_{10} helix, which would finally influence the affinity between the PRS1 and the inhibitor ADP.

Inhibitor Sensitivity Deviation Between wt-PRS1 and D52H-Mutant

To verify the above hypothesis, an ITC measurement had been performed between wt-PRS1 or D52H-mutant and ADP. The results indicated that the dissociation constant (K_d) of ADP to D52H-mutant was 19.7% higher than that of wt-PRS1 (Fig. 5A). The enzyme activity analysis also indicated that, under the 0.15-mM ADP existence conditions, the activity of wt-PRS1 reduced 9.83% and that of D52H-mutant reduced only 1.70%; under the 0.25 mM-ADP existence conditions, the activity reduction of wt-PRS1 was 31.28%, whereas that of D52H-mutant reduced 22.70% (Fig. 5B). The above data showed that the substitution of Asp^{52} by His^{52} enhanced the K_d of ADP to

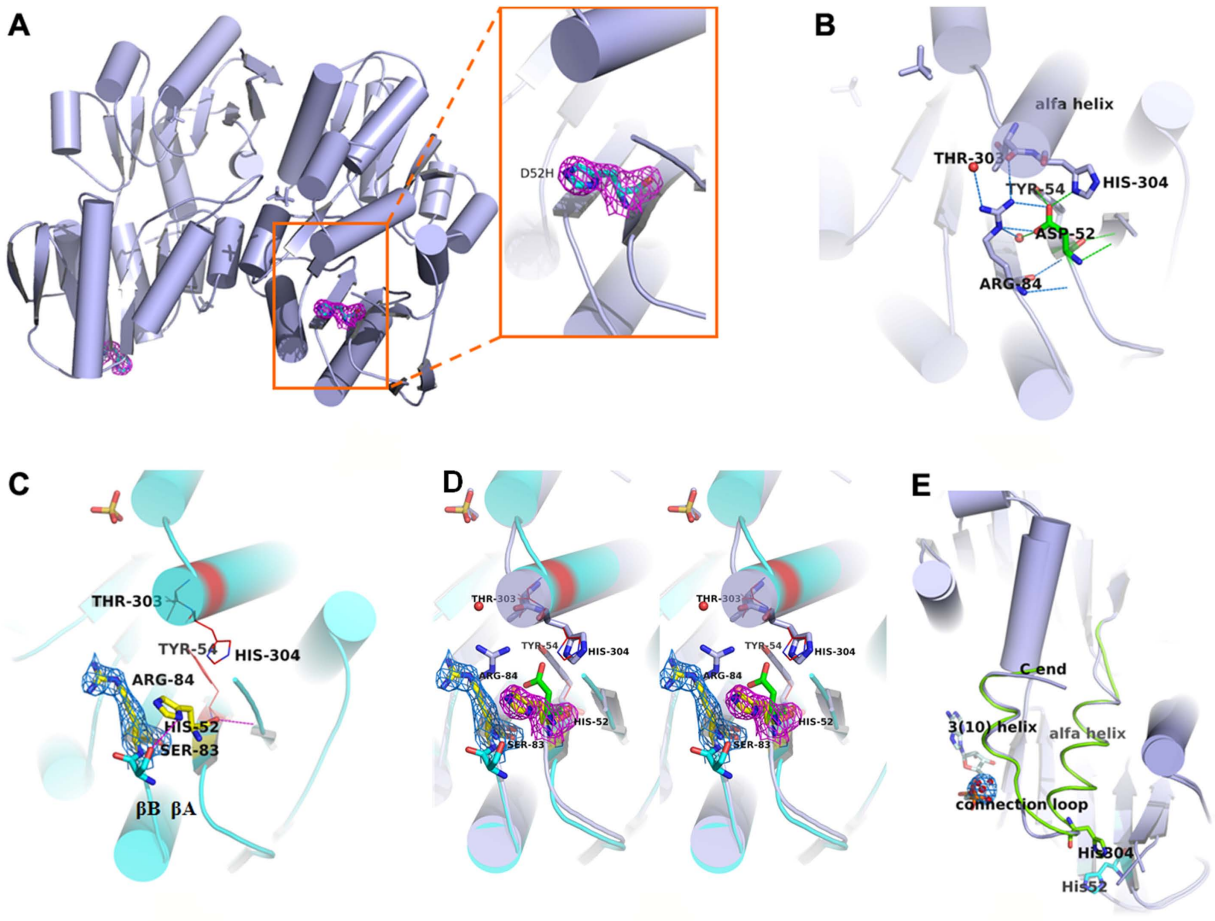

FIG 3

(A) Ribbon representation shows the overall structure of D52H-mutant and the $2F_o - F_c$ electron density around His52. The sigma unit is 1 sigma for all $2F_o - F_c$ maps in this article. (B) The interactional network of Asp52 from wild-type PRS1 with its partners. (C) The disappearance of interactional network of His52 from D52H mutant with its original partners unmoved except the Arg84. The electron density around Arg84 is shown in blue. The newly formed hydrogen bond is shown and labeled as purple dashed line. (D) Stereo view of the detailed conformation changes at the ADP-binding site. The superposition of the interactional networks around the 52-position before and after the histidine substitution. (E) The ADP-binding motif and the structure deviations around His52. The captured SO42[sbond] by our crystal, which represents the moiety of ADP, is shown as ball and sticks with its $2F_o - F_c$ electron density colored blue around it. [Color figure can be viewed in the online issue, which is available at wileyonlinelibrary.com.]

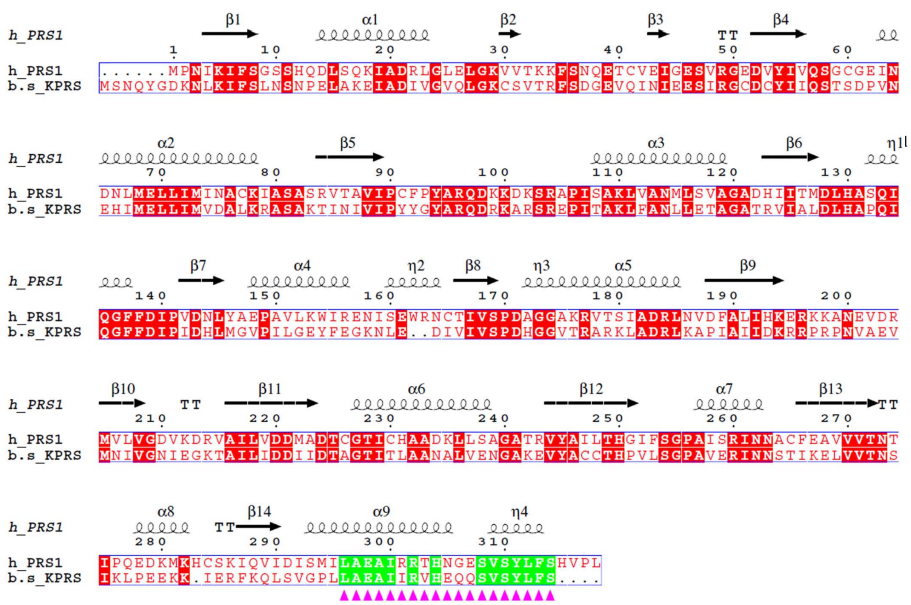

FIG 4

Structure-based sequence alignment of human PRS1 and bsKPRS. Identical residues are shaded in black, whereas those conserved residues for ADP binding are shaded in grey. The black triangles mark the region of the C-terminal a-helix and the 310 helix for ADP binding. [Color figure can be viewed in the online issue, which is available at wileyonlinelibrary.com.]

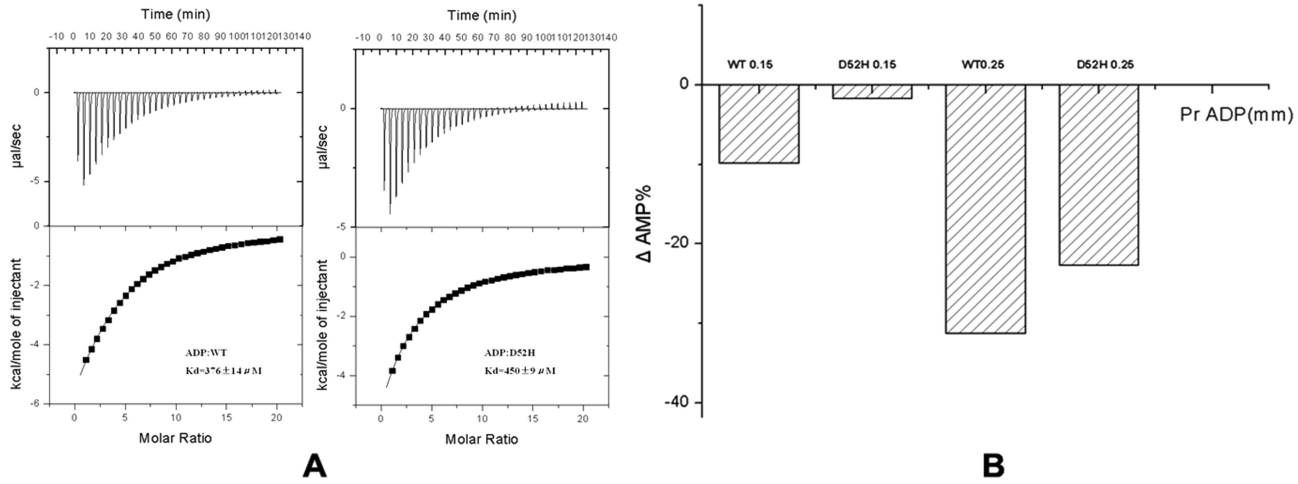

FIG 5 *(A) ITC for inhibitor ADP to both wild PRS1 and D52H-mutant. (B) The resistance to inhibitor ADP of D52H compared with wild-type PRS1. ΔAMP% = ([AMPProtein + n mM ADP] − [AMPProtein+ 0 mM ADP])/(AMPProtein + 0 mM ADP) × 100%.*

PRS1 protein and give it a little resistance (~8%) to the inhibition of ADP. It was consistent with the report that D52H-mutant was resistant to inhibition of activity by ADP (13).

Taking into consideration that, in the human body, only 20% of uric acid is derived from purines ingested in food, but most uric acid comes from our own *in vivo* purine synthesis (29), and the solubility of uric acid is so limited that the normal physiological level is close to the saturation concentration (30), the small structural disturbance which disturbed the inhibitory regulation of human PRS1 in D52H-mutant may increase the uric acid concentrations in patients and finally lead to hyperuricemia and gout.

Acknowledgements

The authors are grateful for the staff at SSRF beamline BL17U for assistance with synchrotron data collection. Financial support for this project was provided by the Chinese Ministry of Science and Technology (grant Nos. 2012CB917200 and 2009CB825500), the Chinese National Natural Science Foundation (grant Nos. 31270014, 31130018, 30900224 and 10979039) and the Science and Technological Fund of Anhui Province for Outstanding Youth (grant No. 10040606Y11).

References

[1] Fox, I. H. and Kelley, W. N. (1972) Human phosphoribosylpyrophosphate synthetase. Kinetic mechanism and end product inhibition. J. Biol. Chem. 247, 2126–2131.

[2] Becker, M. A., Taylor, W., Smith, P. R., and Ahmed, M. (1996) Overexpression of the normal phosphoribosylpyrophosphate synthetase 1 isoform underlies catalytic superactivity of human phosphoribosylpyrophosphate synthetase. J. Biol. Chem. 271, 19894–19899.

[3] Li, S., Lu, Y., Peng, B., and Ding, J. (2007) Crystal structure of human phosphoribosylpyrophosphate synthetase 1 reveals a novel allosteric site. Biochem. J. 401, 39–47.

[4] de Brouwer, A. P., van Bokhoven, H., Nabuurs, S. B., Arts, W. F., Christodoulou, J., et al. (2010) PRPS1 mutations: four distinct syndromes and potential treatment. Am. J. Hum. Genet. 86, 506–518.

[5] Yen, R. C., Raivio, K. O., and Becker, M. A. (1981) Inhibition of phosphoribosylpyrophosphate synthesis in human fibroblasts by 6-methylthioinosinate. J. Biol. Chem. 256, 1839–1845

[6] Lieberman, I., Kornberg, A., and Simms, E. S. (1955) Enzymatic synthesis of pyrimidine nucleotides; orotidine-5′-phosphate and uridine-5′-phosphate. J. Biol. Chem. 215, 403–451.

[7] Preiss, J. and Handler, P. (1958) Biosynthesis of diphosphopyridine nucleotide. II. Enzymatic aspects. J. Biol. Chem. 233, 493–500.

[8] Sperling, O., Eilam, G., Sara Persky, B., and De Vries, A. (1972) Accelerated erythrocyte 5-phosphoribosyl-1-pyrophosphate synthesis. A familial abnormality associated with excessive uric acid production and gout. Biochem. Med. 6, 310–316.

[9] Kim, H. J., Sohn, K. M., Shy, M. E., Krajewski, K. M., Hwang, M., et al. (2007) Mutations in PRPS1, which encodes the phosphoribosyl pyrophosphate synthetase enzyme critical for nucleotide biosynthesis, cause hereditary peripheral neuropathy with hearing loss and optic neuropathy (cmtx5). Am. J. Hum. Genet. 81, 552–558.

[10] de Brouwer, A. P., Williams, K. L., Duley, J. A., van Kuilenburg, A. B., Nabuurs, S. B., et al. (2007) Arts syndrome is caused by loss-of-function mutations in PRPS1. Am. J. Hum. Genet. 81, 507–518.

[11] Liu, X., Han, D., Li, J., Han, B., Ouyang, X., et al. (2010) Loss-of-function mutations in the PRPS1 gene cause a type of nonsyndromic X-linked sensorineural deafness, DFN2. Am. J. Hum. Genet. 86, 65–71.

[12] Roessler, B. J., Golovoy, N., Palella, T. D., Heidler, S., and Becker, M. A. (1991) Identification of distinct PRS1 mutations in two patients with X-linked phosphoribosylpyrophosphate synthetase superactivity. Adv. Exp. Med. Biol. 309B, 125–128.

[13] Becker, M. A., Smith, P. R., Taylor, W., Mustafi, R., and Switzer, R. L. (1995) The genetic and functional basis of purine nucleotide feedback-resistant phosphoribosylpyrophosphate synthetase superactivity. J. Clin. Invest. 96, 2133–2141.
[14] Garcia-Pavia, P., Torres, R. J., Rivero, M., Ahmed, M., Garcia-Puig, J., and Becker, M. A. (2003) Phosphoribosylpyrophosphate synthetase overactivity as a cause of uric acid overproduction in a young woman. Arthritis Rheum. 48, 2036–2041.
[15] de Brouwer, A. P. M., Williams, K. L., Duley, J. A., van Kuilenburg, A. B. P., Nabuurs, S. B., et al. (2007) Arts syndrome is caused by loss-of-function mutations in PRPS1. Am. J. Hum. Genet. 81, 507–518.
[16] Kim, H.-J., Sohn, K.-M., Shy, M. E., Krajewski, K. M., Hwang, M., et al. (2007) Mutations in PRPS1, which encodes the phosphoribosyl pyrophosphate synthetase enzyme critical for nucleotide biosynthesis, cause hereditary peripheral neuropathy with hearing loss and optic neuropathy (cmtx5). Am. J. Hum. Genet. 81, 552–558.
[17] Liu, X., Han, D., Li, J., Han, B., Ouyang, X., et al. (2009) Loss-of-function mutations in the PRPS1 gene cause a type of nonsyndromic X-linked sensorineural deafness, DFN2. Am. J. Hum. Genet. 86, 65–71.
[18] Moran, R., Kuilenburg, A. B., Duley, J., Nabuurs, S. B., Retno-Fitri, A., et al. (2012) Phosphoribosylpyrophosphate synthetase superactivity and recurrent infections is caused by a p.Val142Leu mutation in PRS-I. Am. J. Med. Genet. A 158A, 455–460.
[19] de Brouwer, A. P. M., van Bokhoven, H., Nabuurs, S. B., Arts, W. F., Christodoulou, J., et al. (2010) PRPS1 mutations: four distinct syndromes and potential treatment. Am. J. Hum. Genet. 86, 506–518.
[20] Liu, X., Han, D., Li, J., Han, B., Ouyang, X., et al. (2010) Loss-of-function mutations in the PRPS1 gene cause a type of nonsyndromic X-linked sensorineural deafness, DFN2. Am. J. Hum. Genet. 86, 65–71.
[21] Sperling, O., Persky-Brosh, S., Boer, P., and De Vries, A. (1973) Human erythrocyte phosphoribosylpyrophosphate synthetase mutationally altered in regulatory properties. Biochem. Med. 7, 389–395.
[22] Otwinowski, Z. and Minor, W. (1997) Processing of X-ray diffraction data collected in oscillation mode. Macromol. Crystallogr A 276, 307–326.
[23] CCP 4 (1994) The CCP4 suite: programs for protein crystallography, Acta Crystallogr. D Biol. Crystallogr. 50, 760–763.
[24] Murshudov, G. N., Skubak, P., Lebedev, A. A., Pannu, N. S., Steiner, R. A., et al. (2011) REFMAC5 for the refinement of macromolecular crystal structures. Acta Crystallogr. D Biol. Crystallogr. 67, 355–367.
[25] Adams, P. D., Afonine, P. V., Bunkoczi, G., Chen, V. B., Davis, I. W., et al. (2010) PHENIX: a comprehensive Python-based system for macromolecular structure solution. Acta Crystallogr. D Biol. Crystallogr. 66, 213–221.
[26] Emsley, P. and Cowtan, K. (2004) Coot: model-building tools for molecular graphics. Acta Crystallogr. D Biol. Crystallogr. 60, 2126–2132.
[27] Laskowski, R. A., Rullmannn, J. A., MacArthur, M. W., Kaptein, R., and Thornton, J. M. (1996) AQUA and PROCHECK-NMR: programs for checking the quality of protein structures solved by NMR. J. Biomol. NMR 8, 477–486.
[28] Eriksen, T. A. and Kadziola, A. (2002) Binding of cations in *Bacillus subtilis* phosphoribosyldiphosphate synthetase and their role in catalysis. Structure 271–279.
[29] Gannon, M. C., Nuttall, J. A., Damberg, G., Gupta, V., and Nuttall, F. Q. (2001) Effect of protein ingestion on the glucose appearance rate in people with type 2 diabetes. J. Clin. Endocrinol. Metab. 86, 1040–1047.
[30] Lamontagne, A. E., Jr. (1989) 2,8-Dihydroxyadenine urolithiasis: report of a case in a woman in the United States. J. Urol. 142, 369–370.